NUMERICAL EXPERIMENTS IN 1-D EULER EQUATIONS USING HIGHER ORDER SCHEMES

K.S. Ravichandran*

Abstract

A comparative study of the performance of commonly used, TVD or non-7VD second order accurate numerical algorithms for selected gas dynamic problems governed by 1-D Euler equations is presented.

Introduction

Recently the necessity of ensuring accurate, reliabe and robust resolution of the inviscid solution features governed by the non-linear convection terms of the Euler equations has been *well* appreciated [1,21. The need for this becomes especially important in shock-viscous interaction problems where both excessively smeared but monotone shock profiles as well as steep shock profile with non-physical pre and post-shock oscillations ought to be avoided if computed solution is to be analysed for finer flow structure with confidence. As for as this issue is concerned, one of the examples computed in the present work purports draw attention to the fact that the dividing line between confidence and lack of it in a numerical algorithm, when it comes to interpretation of the computed solution may indeed be very thin. Much effort has lately been spent in tackling these problems and the success of ENONNO type schemes in guaranteeing highly accurate solutions without spurious numerical effects in the solution of inviscid flow problems is very heartening [1-31. Algorithms of the ENO/UNO type are however highly nonlinear (even for linear problems) and also are solution adaptive in the sense that the computational stencil depends on the features present in the evolving solution and so varies from grid point to grid point. For this reason, especially for orders of accuracy higher than 2, these algorithms arc highly computer intensive. While 3-D computations using these algorithms, even for the inviscid case. may be safely ruled out in the context of the available computing power in the country, 2-D computations may be feasible with existing super-minis and parallel computing power either already available or likely to be routinely available in the near future. It therefore becomes important that the performance of these algorithms be assessed for their relative utility in striking the fine balance that we require between economy and feasibility on the one hand and quality and trustworthiness of the computed solution on the other. The present paper is an attempt to study a few algorithms bearing this in mind.

In this paper we present the results of numerical experiments with selected 1-D gas dynamic problems using second order accurate TVD schemes of the flux-difference splitting type [4], the commonly used MacCormack scheme with some additional dissipastion [5], and the ENO/UNO type of algorithms which are suitable for calculations with arbitrary orders of accuracy [3]. Section 2 gives a brief summasry of the numerical schemes used and section 3 discusses the numerical experiments and comparisons.

Work is currently in progress to develop 2-D versions of these codes. It is hoped that similar numerical experiments and comparisons will be presented for the shock reflection and other such problems in the near future.

Numerical Schemes for 1-D Euler Equations

An initial value problem for the Euler equations in conservation form may be formulated as follows.

* CFTD Division, National Aeronautical Laboralor}, Itangaloro560 017.

(2.1a) $\frac{\partial U}{\partial t} + \frac{\partial F}{\partial x} = 0$

(2.1b) $U(x,0) = U_o(x)$

where the conserved variable $U = [\rho, \rho q, e]^T$, the flux $F = [\rho q, p+\rho q^2, q(e+p)]^T$, pressure $p = (\gamma-1)\{e-\frac{1}{2}\rho q^2\}$, ρ=density, q=gas sped and e=total energy. The sound speed $c=\gamma p/\rho$ and total enthalpy $H=(e+p)/\rho=c^2/(\gamma-1)+q^2/2$.

The eigenvalues of the Jacobian of the flux vector F are q-c,q,q+c. The Jacobian and the normalized right and left eigenvector matrices are given below.

(2.2a) $A = \frac{\partial F}{\partial U} = \begin{bmatrix} 0 & 1 & 0 \\ (\gamma-3)/2\ q^2 & (3-\gamma)q & \gamma-1 \\ -\gamma qe/\rho+(\gamma-1)q^3 & \gamma e/\rho-1.5(\gamma-1)\ q^2 & \gamma q \end{bmatrix}$

(2.2b) $R = \begin{bmatrix} 1 & 1 & 1 \\ q-c & q & q+c \\ H-qc & q^2/2 & H+qc \end{bmatrix}$

(2.2c) $R^{-1} = \frac{1}{2} \begin{bmatrix} b_1+q/c & -b_2q-1/c & b_2 \\ 2(1-b_1) & 2b_2q & -2b_2 \\ b_1-q/c & -b_2q+1/c & b_2 \end{bmatrix}$

$b_2 = (\gamma-1)/c^2, \quad b_1 = .5(\gamma-1)q^2/c^2 = 0.5b_2q^2$

A general conservative discretization of (2.1a) is given by,

(2.3) $U_j^{n+1} = U_j^n - \lambda (\hat{F}_{j+\frac{1}{2}} - \hat{F}_{j-\frac{1}{2}})$

where the numerical flux $\hat{F}(U^n_{j-r}, \ldots, U^n_{j+s+1})$, r=0,1, etc. is consisent iff $\hat{F}(U,U, \ldots U) = F(U)$. All the schemes used in the present paper can be cast in the conservative form (2.3). We therefore now proceed to specify the numerical fluxes for each of these schemes. In all the schemes, wherever averages are encountered at cell interfaces (half grid points), a simple arithmetic average has been used.

(1) Second order symmeric TVD scheme (TVDSYM) [4].

(2.4a) $\hat{F}_{j+\frac{1}{2}} = \frac{1}{2} [F_j + F_{j+1} + R_{j+\frac{1}{2}} \Phi_{j+\frac{1}{2}}]$

(2.4b) $\Phi_{j+\frac{1}{2}} = [\phi^1, \phi^2, \phi^3]^T_{j+\frac{1}{2}}$

(2.4c) $\phi^i_{j+\frac{1}{2}} = -\lambda(c^i_{j+\frac{1}{2}})^2\ \hat{Q}^i_{j+\frac{1}{2}} - \psi(c^i_{j+\frac{1}{2}})\ (\alpha^i_{j+\frac{1}{2}} - \hat{Q}^i_{j+\frac{1}{2}})$

(2.4d) $\alpha^i_{j+\frac{1}{2}} = (R^{-1})_{j+\frac{1}{2}}\ (U_{j+1} - U_j)$

(2.4e) $\psi(z) = |z| \text{ if } |z| > 2\varepsilon$

$= (z^2 + 4\varepsilon^2)/4\varepsilon \text{ if } |z| < 2\varepsilon$

(2.4f) $\hat{Q}^i_{j+\frac{1}{2}} = \text{minmod}\ (\alpha^i_{j+\frac{1}{2}}, \alpha^i_{j+3/2})$

(2) Second order upwind TVD scheme (HARYEE) [4].

(2.5a) $\hat{F}_{j+\frac{1}{2}} = \frac{1}{2} [F_j + F_{j+1} + R_{j+\frac{1}{2}} \Phi_{j+\frac{1}{2}}]$

(2.5b) $\Phi_{j+\frac{1}{2}} = [\phi^1, \phi^2, \phi^3]^T\ j_{+\frac{1}{2}}$

(2.5c) $\phi^i_{j+\frac{1}{2}} = \sigma(c^i_{j+\frac{1}{2}})\ (g^i_{j+1} + g^i_j) - \psi\ (c^i_{j+\frac{1}{2}} + \gamma^i_{j+\frac{1}{2}})\ \alpha^i_{j+\frac{1}{2}}$

(2.5d) $\alpha^i_{j+\frac{1}{2}} = (R^{-1})_{j+\frac{1}{2}}\ (U_{j+1} - U_j)$

(2.5e) $\psi(z) = |z| \text{ if } |z| > 2\varepsilon$

$= (z^2 + 4\varepsilon^2)/4\varepsilon \text{ if } |z| < 2\varepsilon$

(2.5f) $\sigma(z) = \frac{1}{2} (\psi(z) - \lambda z^2)$

(2.5g) $g^i_j = \text{minmod}\ (\alpha^i_{j-\frac{1}{2}}, \alpha^i_{j+\frac{1}{2}})$

(2.5h) $\gamma^i_{j+\frac{1}{2}} = \sigma(c^i_{j+\frac{1}{2}})\ (g^i_{j+1} - g^i_j) / \alpha^i_{j+\frac{1}{2}} \text{ if } \alpha^i_{j+1/2} \neq 0$

$= 0 \text{ otherwise}$

(3) Harten's second order TVD scheme (ULT1) [6].

(2.6a) $\hat{F}_{j+\frac{1}{2}} = \frac{1}{2} [F_j + F_{j+1} - 1/\lambda\ R_{j+\frac{1}{2}} \Phi_{j+\frac{1}{2}}]$

(2.6b) $\Phi_{j+\frac{1}{2}} = [\phi^1, \phi^2, \phi^3]^T_{j+\frac{1}{2}}$

(2.6c) $\phi^i_{j+\frac{1}{2}} = -\sigma(g^i_{j+1} + g^i_j) + \psi(\lambda c^i_{j+\frac{1}{2}} + \gamma^i_{j+\frac{1}{2}})\ \alpha^i_{j+\frac{1}{2}}$

(2.6d) $\alpha^i_{j+\frac{1}{2}} = (R^{-1})_{j+\frac{1}{2}}\ (U_{j+1} - U_j)$

(2.6e) $\psi(z) = |z| \text{ if } |z| > 2\varepsilon$

$= (z^2 + 4\varepsilon^2)/4\varepsilon \text{ if } |z| < 2\varepsilon$

(2.6f) $g^i_j = \text{minmod}\ (\dot{g}^i_{j+\frac{1}{2}}, \dot{g}^i_{j+\frac{1}{2}})$

(2.6g) $\gamma^i_{j+\frac{1}{2}} = (g^i_{j+1} - g^i_j) / \alpha^i_{j+\frac{1}{2}} \text{ if } \alpha^i_{j+\frac{1}{2}} \neq 0$

$= 0 \text{ otherwise}$

(2.6h) $g^i_{j+\frac{1}{2}} = \frac{1}{2}[\psi(\lambda c^i_{j+\frac{1}{2}}) - (\lambda c^i_{j+1/2})^2]\ \alpha^i_{j+\frac{1}{2}}$

(4) MacCormack scheme with artificial dissipation [5].

(2.7a) $\hat{\bar{F}}_{j+\frac{1}{2}} = \frac{1}{2}[\bar{\bar{F}}_{j+1} + \bar{\bar{F}}^n_j]$

(2.7b) $\bar{\bar{F}}^n_j = F^n_j + T^n_j,\ F^n_j = F(U^n_j)$

(2.7c) $T^n_j = \alpha\ \sigma^n_j\ |\ \frac{p_{j+1} - 2p_j + p_{j-1}}{p_{j+1} + 2p_j + p_{j-1}}\ |\ (U^n_{j+1} - U^n_j)$

(2.7d) $\bar{\bar{F}}_j = \bar{\bar{F}}^n_j + \bar{\bar{T}}^n_j,\ \bar{\bar{F}}^n_j = F(\bar{U}^n_j),\ \sigma^n_j = |q^n_j| + c^n_j$

(2.7e) $\bar{U}^n_j = U^n_j - \lambda(\bar{\bar{F}}^n_j + \bar{\bar{F}}^n_{j-1})$

(2.7f) $\bar{T}^n_j = \alpha\ \bar{\sigma}^n_j\ |\ \frac{\bar{p}_{j+1} - 2\bar{p}_j + \bar{p}_{j-1}}{\bar{p}_{j+1} - 2\bar{p}_j + \bar{p}_{j-1}}\ |\ (\bar{U}^n_{j+1} - \bar{U}^n_j)$

The minmod function takes that value of a list of arguments which is least in absolute value if all arguments are of same sign and zero otherwise. In (2.7a and f), the artificial viscosity term $\bar{T}_{j+1}$ requires the computation of $\bar{U}_j$ for j=j+1 and j+2. For reasons of economy we however do not compute thie intermediate state $\bar{U}$ and corresponding $\bar{p}$ for j=j+2. but use the unbarred quantities for the same grid points. The constant α is restricted to $0 \leq \alpha \leq 1$.

(5) UNO scheme of Harten et. al. [3].

This scheme, which is essentially Godunov's scheme extended to arbitrary orders of accuracy, is too complex to be described here in detail. The scheme has two main component algorithms: (i) Given cell averages, to reconstruct a non-oscillatory interpolant of the primitive function and (ii) construction of a solution in the small using a Cauchy-Kovalewsky procedure with the reconstructed distribution as initial data. The scheme can also be written in the general conservative form given by (2.3). For complete details the reader may see [3].

Numerical Experiments and Discussions

The following problems have been selected for numerical computations and comparisons. The first two are simple Reimann problems. The third is the so-called shock-turbulence interaction model problem and is in a sense a generalized Riemann problem or a Riemann problem whose solution has a richer structure than the centered simple wave solutions one is familiar with. The last is a variation of the third problem and is included here as a more practical case as well as to illustrate the pitfalls one most guard against while interpreting numerical solutions.

For the first two problems the initial data for the left and rights states respectively are

(1) Lax : $U_l = [1.0,0.0,2.5]^t$, $U_r = [0.125,0.0,0.25]^t$

(2) Sod : $U_l = [0.445,0.311,8.928]^t$,

$U_r = [0.5,0.0,1.4275]^t$

The intial data for the shock-turbulence (density wave) interaction model is given in terms of primitive variables as,

$\rho_l = 3.857143,\ q_l = 2.629367,\ p_l = 10.333333 \qquad -6 \leq x \leq -4$

$\rho_l = 1.0 + \varepsilon\sin(\pi\omega x),\ q_l = 0.0,\ p_r = 1.0 \qquad -4 \leq x \leq 4$

$\rho_l = 1.0,\ q_l = 0.0,\ p_r = 1.0 \qquad 4 \leq x \leq 6$

The initial data for the second shock-turbulence interaction model is obtained by replacing the density wave by a velocity wave. The data then is,

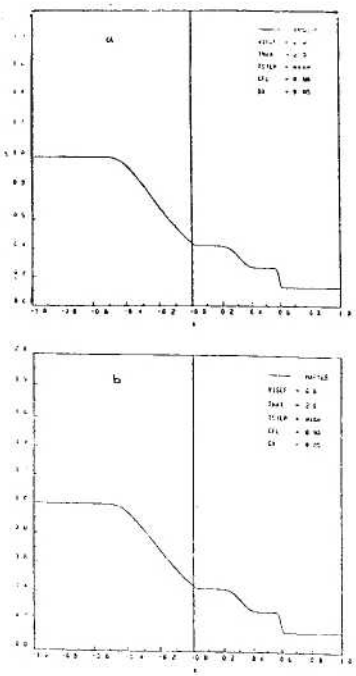

Fig. 1. Lax's Riemann Problem

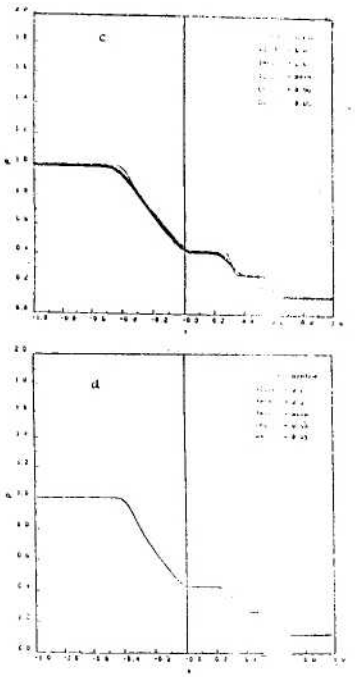

Fig. 1. Lax's Riemann Problem

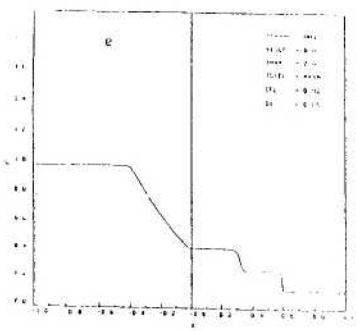

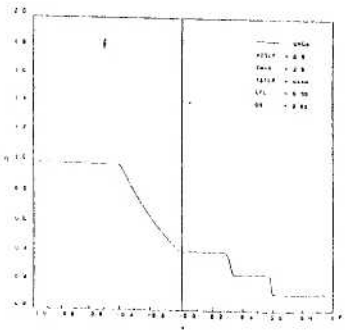

Fig. 1. Lax's Riemann Problem

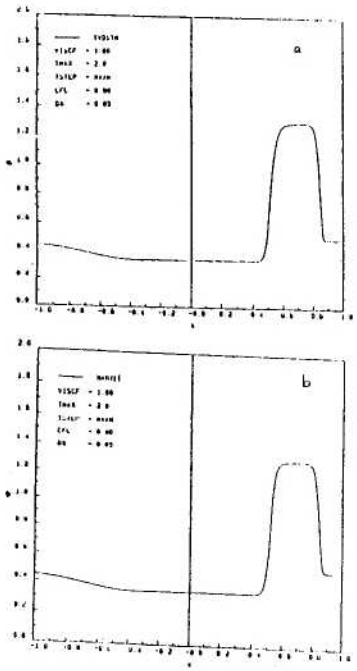

Fig. 2. Sod's Riemann Problem

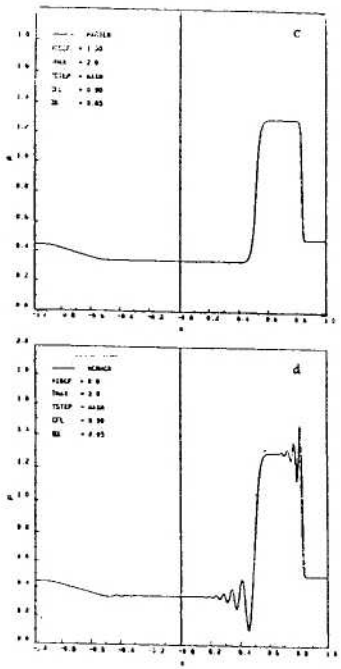

Fig. 2. Sod's Riemann Problem

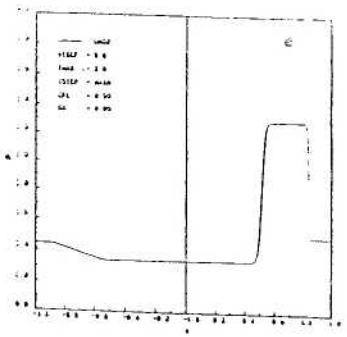

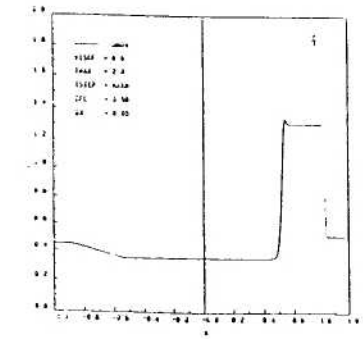

Fig. 2. Sod's Riemann Problem

$\rho_l = 3.857143,\ q_l = 2.629367,\ p_l = 10.333333 \qquad -6 \le x \le -4$

$\rho_r = 1.0 + \varepsilon\sin(\pi\omega x),\ p_r = 1.0 \qquad -4 \le x \le 4$

$\rho_r = 1.0,\ q_r = 0.0,\ p_r = 1.0 \qquad 4 \le x \le 6$

The idea behind this modification is that in practice velocity and pressure oscillations are more likely in quiscent medium which may be considered to be incompressible so that density is held constant.

All computations are carried out in the interval $-6 \le x \le 6$ unless otherwise mentioned. For plotting purposes the normalized interval is $-1 \le x \le 1$. Computations were done for t=2.0 with CFL number-0.9 for the first two Riemann problems. Computations for the shock turbulence interaction model problem were carried out till t=2.5 with CFL number = 0.9 except in two cases (mentioned in the text) for which CFL number=1.

Figs. 1a to f show the computed density distribution of Lax's Riemann problem in the solution to which a sonic condition occurs at the tail of the rarefaction fan propagating to the left. We note that in spite of second order accuracy, the first two schemes, namely the symmetric TVD scheme (TVDSYM) and the Harten-Yee Upwind (HARYEE) TVD scheme, produce a smeared rarefaction fan as well as a contact discontinuity, indicative of excessive dissipastion in the schemes. This may be due to a bad choice of the flux limiter. However other flux limiters have not been so far tried. Fig. 1c where the TVDSYM solution is compared with the ULTI solution gives an idea of the dissipation present in these second order TVD schemes. The best compromise between computational economy and accuracy seems to be provided by Harten's second order TVD scheme (ULTI) [6]. This solution, plotted in Fig. 1d, shows a sharper resolution of the head and tail end of the rarefaction fans well as a sharp transition across the contact. In ref. [6] Harten discusses the ways for improved resolution of the contact. MacCormack's scheme fails to compute this case (numerically induced oscillations cause cavitation to occur on the right state because of the low values of the density there) even with artificial dissipation. In fact our experience with the use of artificial dissipation in MacCormack scheme has been that it worsens the performance of the scheme. In any case it does not help at all when the specific cause of the failure of the scheme is cavitation due to numerical oscillations. Figs. 1e and f respectively show the density distribution obtained with second and fourth other UNO schemes. The second order scheme of the UNO type takes more CPU time than the other second order schemes because of the adaptive stencil strategy. The results of course are slightly better too. The fourth order UNO computation though better in terms of accuracy and resolution, is subject to the law of diminishing marginal returns. Higher order computations with the UNO scheme is however useful when the computed solution has more structure than the simple Riemann problems as will be seen below in the third and fourth examples.

Figs. 2a to f show the solutions from these schemes for Sod's Riemann problem. Though no sonic points are involved in the solution to this problem, there is a build up of density across the right moving contact. We note that in general the remarks made in relation to the previous problem apply in this case too except that the resolution of the contact by TVDSYM and HARYEE schemes is comparable to that of ULTI. We also note that MacCormack's scheme succeeds in computing this case in spite of severe oscillations and without any artificial dissipation. Note that there are no oscillations ahead of the discontinuities (shock or contact), in the MacCormack solution. This explains why the scheme succeeds in computing the next example wherein the shock is stronger and the problem appears to be prima facie more difficult. Fig. 2f shows a small overshoot ahead of the contact in the fourth order UNO solution. This is not surprising since the UNO schemes do permit $O(h^r)$ oscillations in the computed solutions in the vicinity of discontinuities.

The shock-turbulence interaction model is more interesting for the richer structure of its solution. We note that in the absence of density oscillations on the right, the shock moves at constant speed $M_s = 3$, to the right. With ε=0.1 and ω=1, we have 4 waves on the right at time t=0, see Fig. 3a. The computation is carried on till t=2.5 when the shock has passed completely through the oscillatory region. The results obtained with various schemes are plotted in Figs. 3c to h. To study the detailed structure of the evolving flow, we have shown in Fig. 3b, the density distribution at t=2 obtained from the fourth order UNO scheme with Δx=0.025. At this time the shock has not completley crossed the wavy density region on the right.

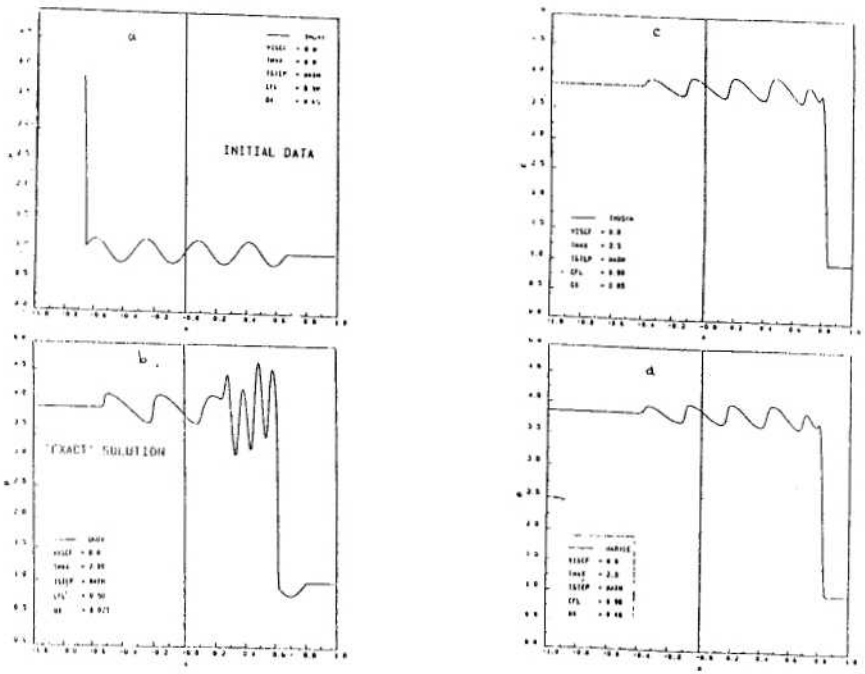

Fig. 3. Mach 3 Shock/Density Wave Interaction

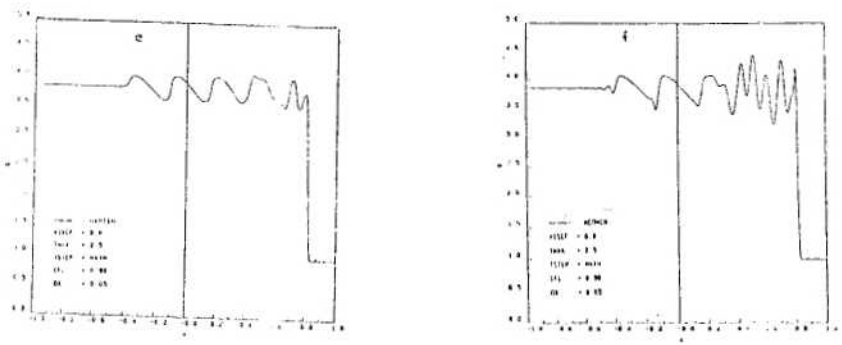

Fig. 3. Mach 3 Shock/Density Wave Interaction

This numerical solution, if regarded as exact or atleast close to being so, shows that the flow behind the shock has two distinct regions. The train of supersonic to supersonic shocks, on the left of the Mach 3 shock is due to the genuinely non-linear acoustic wave family corresponding to the eigenvalue q-c. The shocks are connected to one another by rarefaction fans. Note that the formation of each shock corresponds to the increasing segment (decreasing in the flow direction when viewed from the shock coordinate frame) of density in the oscillatory region ahead of the shock. In contrast to the scalar conservation law wherein, for a convex flux function, the decreasing portion of the initial distribution steepens to form a shock, in the case of Euler equations the increasing segment of the density distribution steepens to form a shock. We also note that the number of shocks exactly corresponds to the number of increasing segments of density (three and half to be precise!). The last shock (that which is closest to the Mach 3 shock) is connected to a region of very steep but regular oscillations in the density signifying a solution domain which corresponds to the wave family q or what is commonly referred to as the entropy wave. We do not see a distinct region corresponding to the eigenvalue q+c because the Mach 3 shock and this region are merged together. In the discussion that follows, each scheme will be evaluated in the light of what has been said above about the solution structure.

Figs. 3c to e show the computed solutions using respetively the TVDSYM, HARYEE and ULTI schemes. We note that the TVDSYM and HARYEE scheme solutions are almost indistinguishable. More importantly the excessive dissipation in these schemes has almost completely smeared out the solution region corresponding to the entropy wave and it appears as though there is only one flow region corresponding to the q-c eigenvalue, comprising of four or four and a half shocks. Clearly the correlation of the kind mentioned above cannot be revealed by these schemes. Harten's ULTI scheme performs slightly better in this respect in the sense that it indicates that there are indeed two distinct solution regions behind the shock, although it fails to resolve the entropy wave region adequately. Fig. 3f and g show the MacCormack solution obtained with artificial dissipation coefficient 0. and 0.2 respectively. Note the kink in the rarefaction fan connecting the weak shocks on the left. While the oscillations at the tail of the shock train is acceptably small the overshoot behind the Mach 3 shock apparently increases with more dissipation see Figs. 3f and g. The merit of the scheme is that it resolves the entropy wave region adequately albeit with an error in the phase (as compared with the UNO4 solution). Computations with higher dissipation coefficient leads to larger oscillations and ultimately breakdown of the algorithm. This confirms the observation made earlier that artificial dissipation in MacCormack scheme does not seem to give any advantage atleast for unsteady computations. Fig. 3h finally shows the second order UNO solution which matches the fourth order computation as far as solution details are concerned. The amplitude of the entropy wave however is significantly uncerpredicted.

In Figs. 4d to i we present the results for the shock-velocity wave interaction. The initial data for this problem is shown in Fig. 4a. Note that, since the absolute value of the Mach number is plotted, two successive oscillations correspond to actually one wave length.

Firstly, to compute the exact solution, we repeat the computation with grid size and CFL number identical with the 'exact' computation for the prevous case, viz. Δx=0.025 and CFL number=1.0. Fig. 4b shows the computed density, Mach number and pressure distributions at t=2. What immediately strikes the eye in this figure is that the pressure distribution shows large oscillations suggestive of 'randomness'. Recall that in the shock-density wave interaction problem, Fig. 3b, an identical computation resulted in a solution that was not only very smooth but also gave no inkling of any hidden numerical errors. (In fact computation on a further halved grid with same CFL number gave strong evidence that the solution was likely to converge with $\Delta x \rightarrow 0$). In the light of this experience and given the strong non-linearity of the governing equations, it is very tempting to regard the computed solution region behind the shock as genuine and interpret it as indicative of the onset of randomness or chaos. Since the scheme is essentially non-oscillatory, the only check to rule out numerically caused spurious randomness was to make sure that the computation was carried out well within the stability bound of the algorithm.

For the UNO algorithm in question, the stability limit is CFL number $\leq$ 1. It was therefore decided to repeat the computation for CFL number 0.9. The results are plotted in Fig. 4c and it is seen immediately that the oscillations seen in the previous figure were caused by mild numerical instabilities and are not to be attributed to the flow itself.

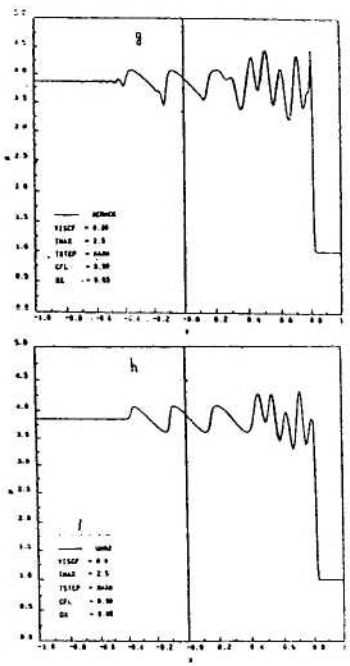

Fig. 3. Mach 3 Shock/Density Wave Interaction

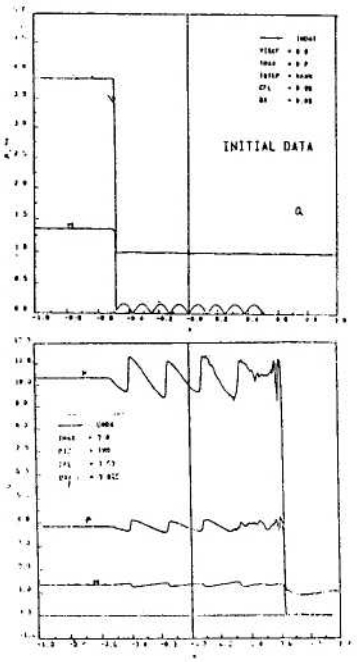

Fig. 4. Mach 3 Shock/Velocity Wave Interaction

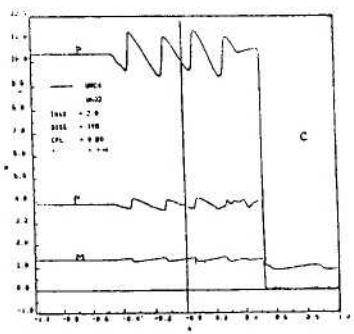

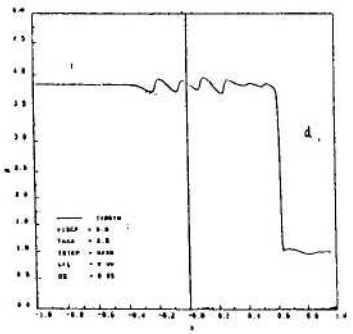

Fig. 4. Mach 3 Shock/Velocity Wave Interaction

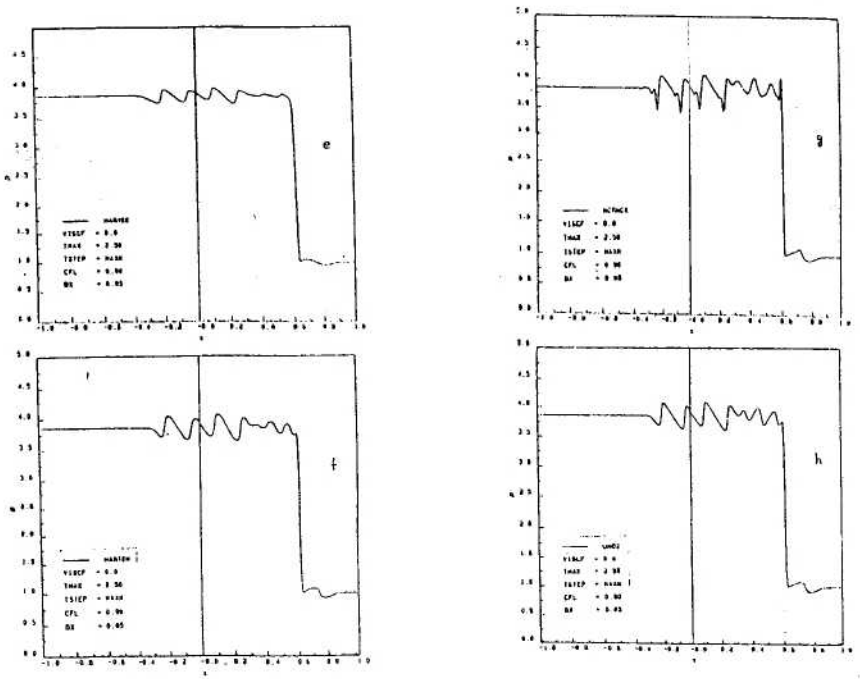

Fig. 4. Mach 3 Shock/Velocity Wave Interaction

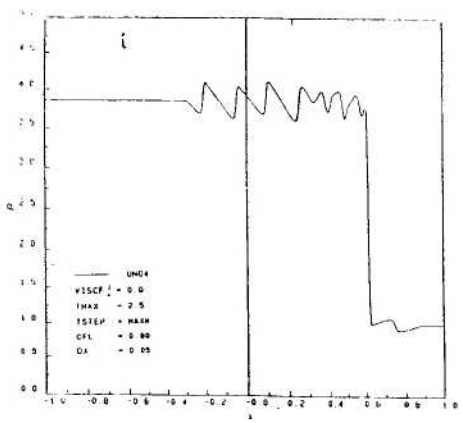

Fig. 4. Mach 3 Shock/Velocity Wave Interaction. UNO4 Scheme

The remarks made above at first sight may seem contrived and unnecessary although it draws attention to the caution one must exercise while intepreting numerical results. One might say,"well, this is nothing new". In reply we make the following remarks: Firstly we note that in the absence of high accuracy algorithms belonging to the ENO/UNO family, we could not even have posed the question of whether the computed flow could be interpreted at face value. The only option in such a situation is that. when confronted with computed results that are contrary to expectations, these should be attributed to numerical error and ignored. For instance, the MacCormack scheme produced a kink in the rarefaction fan between two shocks but this feature (quite correctly bur for no known reason) is immediately ignored and no physical significance is attached to it. Secondly, with monotone algorithms which guarantee the non-generation of spurious oscillations, the computed solution may still be unrepresentative because of poor resolution as seen In

Figs. 3c to e and Figs. 4d to f. Here again we are unable to interpret the solution, but this time for lack of information or too little of it. It is therefore only when we can guarantee high resolution with non-generation of non-physical, spurious numerical features, that we see can pose the question of interpretation of the finer features that may be revealed in a computed solution. In the present case the combination of high accuracy with resolution that is guaranteed by the ENO/UNO type algorithms not only enabled us to raise an interesting question but also answer the same in a definitive manner.

Going back to Fig. 4c, we note that the flow region behind the Mach 3 shock is similar to that encountered in the previous model. The sueprsonic to supersonic shocks on the left are of similar strength as in the previous case, but there is a noticeable quarter wave length shift in the phase. There is also the flow region associated with the entropy wave just behind the Mach 3 shock. The amplitude of the oscillations in this case is however much smaller. A feature of this model problem is the weak shock associated with the q+c eigenvalue, upstream of the Mach 3 shock. The latter being faster, should eventually overtake the weak right running shock. It is not clear whether the passing of this shock behind the Mach 3 shock will result in another shock being added to the shock train on the left (in which there are already 4).

Comparing results from the other schemes to this 'exact' solution, we see from Figs. 4d and e that the TVDSYM and HARYEE completely fail to resolve the entropy wave region, besides producing smeared shock transitions. The ULT1 scheme of Harten, Fig. 3f, gives an inkling of the flow behind the Mach 3 shock. The MacCormack scheme, as in the previous case, does produce two distinct flow regions but with kinks and oscillations, Fig. 4g. Note that this computation has been done without any additional explicit artificial dissipation. Lastly the UNO2 and UNO4 solutions adequately resolve the flow as seen in Figs. 4h and i.

Conclusions

Numerical experience with selected higher order TVD/UNO or non-TVD schemes for the I-D Euler equations show that even without the complexity of flow associated with multi-dimensions, many flow features need to be adequately resolved without introducing spurious numerically generated errors even for qualitative understanding of the computed flow picture. For this reason high order non-oscillatory algorithms currently under development, may be essential for analysing complex flow fields in multi-dimensions.

Acknowledgement

This work was done as part of the Indo-Soviet ILTP programme and is supported by the department of Science & Technology, Govt. of India.

References

1. Shu, C.W. and Osher S., "Efficient Implementation of Essentially Non-Oscillatory Shock Capturing Schemes II", J. Comp. Phys., V83, p32, (1989).

2. Shu, C.W., et. al., "High-Order ENO Schemes Applied to Two and Three Dimensional Compressible Flow", NASA CR 187562, ICASE Rep. No. 91-38, (1991).

3. Harten, A., et. al., "Uniformly High Order Accurate Essentially Non-Oscillatory Schemes", J. Comp. Phys., V71, p231, (1987).

4. Yex, H., "A Class of High-Resolution Explicit and Implicit Shock-Capturing Methods", NASA TM 101088,(19890.

5. MacCormack, R.W. and Baldwin, B.S. "A Numerical Method for Solving the Navier-Stokes Equations with Application to Shock-Boundary Layer Interactions", AIAA Paper No. 75-1, (1975).

6. Harten, A., "High Resolution Schemes for Hyderbolic Conservation Laws", J. Comp. Phys., V49, p357, (1983).